J. Fluid Mech. (2006), *vol.* 567, *pp.* 1–26.
doi:10.1017/S0022112006002400 Printed in the United Kingdom

Physical interpretation of unstable modes of a linear shear flow in shallow water on an equatorial beta-plane

By HIROSHI TANIGUCHI† AND MASAKI ISHIWATARI

Faculty of Environmental Earth Science, Hokkaido University, Sapporo 060-0810, Japan

(Received 10 September 2004 and in revised form 27 February 2006)

Unstable modes of a linear shear flow in shallow water on an equatorial β-plane are obtained over a wide range of values of a non-dimensional parameter and are interpreted in terms of resonance between neutral waves. The non-dimensional parameter in the system is $E \equiv \gamma^4/(gH\beta^2)$, where γ, g, H and β are the meridional shear of basic zonal flow, gravitational constant, equivalent depth and the north–south gradient of the Coriolis parameter, respectively. The value of E is varied within the range $-2.50 \leqslant \log E \leqslant 7.50$.

The problem is solved numerically in a channel of width $5\gamma/\beta$. The structures of the most unstable modes, and the combinations of resonating neutral waves that cause the instability, change according to the value of E as follows. For $\log E < 2.00$, the most unstable modes have zonally non-symmetric structures; the most unstable modes for $\log E < 1.00$ are caused by resonance between equatorial Kelvin modes and continuous modes, and those for $1.00 \leqslant \log E < 2.00$ are caused by resonance between equatorial Kelvin modes and westward mixed Rossby–gravity modes. The most unstable modes for $\log E \geqslant 2.00$ have symmetric structures and are identical with inertially unstable modes. Examinations of dispersion curves suggest that non-symmetric unstable modes for $1.00 \leqslant \log E < 2.00$ and inertially unstable modes for $\log E \geqslant 2.00$ are the same kind of instability.

1. Introduction

It has been considered that inertial instability occurs in planetary atmospheres. Pancake structures found in the terrestrial equatorial stratopause are considered to be an inertial instability phenomenon (Hitchman *et al.* 1987; Hayashi, Shiotani & Gille 1998). The reason is that pancake structures have similar characteristics to the zonally non-symmetric unstable modes which Dunkerton (1983) obtained and argued to be inertial instability. Using general circulation models for Venus and Titan, it was shown that the equatorial regions of both atmospheres can be inertially unstable (Allison, Del Genio & Zhou 1994). In addition, for the Jovian planets it was argued that inertial instability contributes to maintaining the upper-layer zonal wind profiles through the mixing of angular momenta (Allison, Del Genio & Zhou 1995).

Although, based on the results of Dunkerton (1983), pancake structure is considered to be caused by inertial instability, it has not been determined whether the zonally

† Present address: Disaster Prevention Research Institute, Kyoto University, Uji, Kyoto 611-0011, Japan.

non-symmetric unstable modes that he obtained can be considered to be the same kind of instability as the symmetric inertial instability. Inertial instability in the equatorial region has been addressed by Dunkerton (1981) and by Stevens (1983). With a zonally symmetric basic flow on an equatorial β-plane, they showed that symmetric inertial instability occurs if there exists a region where the product of the Coriolis parameter and potential vorticity is negative (hereinafter, referred to as the 'inertially unstable region'). Following these studies, several authors investigated zonally non-symmetric unstable modes. Boyd & Christidis (1982) considered that the equatorial Kelvin wave is destabilized in equatorial shear flow, and that the instability of the Kelvin wave in strong shear flow corresponds to inertial instability. Dunkerton (1983) showed that the non-symmetric modes have large amplitudes in inertially unstable regions, and regarded the modes as inertially unstable modes. Clark & Haynes (1996), through an asymptotic expansion in wavenumber, obtained a condition that non-symmetric modes dominate over symmetric modes. However, a physical interpretation of the correspondences of the destabilized Kelvin wave (Boyd & Christidis 1982) and non-symmetric modes (Dunkerton 1983; Clark & Haynes 1996) to symmetric inertially unstable modes are not given in those papers.

Moreover, although there is the possibility that inertial instability occurs in many planetary atmospheres, no attempts have been made to explore unstable modes over a wide range of parameters. It is unclear whether there exists an unstable mode other than the destabilized Kelvin wave discussed by Boyd & Christidis (1982). In systems involving an equatorial region and a higher latitudinal region, many types of unstable mode were found (Winter & Schmitz 1998; Iga & Matsuda 2005). However, little interpretation of these unstable modes was given in previous studies, since their basic states were complicated because they attempted to model real atmospheres.

Unstable modes are often interpreted by the use of the concept that an instability is caused by interaction between neutral waves satisfied with certain conditions (Cairns 1979; Hayashi & Young 1987; Iga 1999*c*). According to the concept, an unstable mode is considered to result from the resonance of two neutral waves which have opposite signs of pseudomomenta and the same values of phase speed. Exchange of pseudomomenta between neutral waves causes the growth of an unstable mode, while pseudomomentum of the whole system is conserved. When the resonance of neutral waves occurs, their dispersion curves intersect at a certain wavenumber (Hayashi & Young 1987). For the wavenumber in a stable region, there exist dispersion curves of two neutral waves with opposite signs of pseudomomenta. For a wavenumber with which instability occurs, dispersion curves of the growing mode and the decaying mode coincide with each other. Consequently, observation of dispersion curves enables us to identify the neutral waves which cause instability. This concept successfully yields physical interpretations for unstable modes in one-layer problems (Kubokawa 1986; Hayashi & Young 1987) and in two-layer problems (Iga 1993, 1997). Not only non-singular modes, but also singular (i.e. continuous) modes resonate with other modes and yield unstable modes. Iga (1999*a*) showed that a superposition of continuous modes yields unstable modes by resonating with neutral modes in the critical-layer instability problem. The unstable modes obtained by him are caused by resonance between the first Poincaré modes and a superposition of continuous modes in a two-layer model. The signs of pseudomomenta for neutral modes and continuous modes are, respectively, determined by the gradient of the dispersion curve and by the gradient of the potential vorticity of a basic flow (Iga 1999*a*,*b*).

In this paper, unstable modes in a linear shear flow on an equatorial β-plane are obtained over a wide parameter range by solving an eigenvalue problem. Based on the

results of the eigenvalue problem, interpretations of the unstable modes are given by the use of the concept of resonance between neutral waves (Hayashi & Young 1987; Iga 1995). In light of these results, we discuss whether the non-symmetric unstable modes obtained by Boyd & Christidis (1982) and Dunkerton (1983) are similar to inertially unstable modes obtained by Dunkerton (1981) and Stevens (1983).

This paper is organized as follows. The system and basic equations are explained in § 2. Section 3 presents the calculated eigenvalues and the structures of unstable modes. Dispersion curves of unstable modes are examined according to the concept of resonance between neutral waves in § 4. In §§ 5 and 6, respectively, resonating equatorial Kelvin modes and resonating mixed Rossby–gravity modes are examined. In § 7, the results are summarized, and the correspondence of non-symmetric unstable modes to symmetric inertially unstable modes is discussed.

2. Basic equations

Our basic equations are the horizontal structure equations of a primitive system using an equatorial β-plane approximation (Stevens 1983); dissipation is excluded. At both the north and south boundaries, meridional velocities are set to zero. The x- and y-axes are along the longitudinal and meridional directions, respectively. The equator is located at $y=0$. Our system is equivalent to a shallow-water channel on an equatorial β-plane.

By expanding variables in zonal harmonics in the same manner as Dunkerton (1993), the non-dimensional perturbation equations linearized about the linear shear flow are:

$$-(\omega - k\bar{u})u + (1-y)\,v = -k\phi, \tag{2.1}$$

$$(\omega - k\bar{u})v + yu = -\frac{\partial \phi}{\partial y}, \tag{2.2}$$

$$-(\omega - k\bar{u})\phi + \frac{1}{E}\left(ku + \frac{\partial v}{\partial y}\right) = 0, \tag{2.3}$$

where $\bar{u}(y)$, u, v and ϕ are the basic zonal velocity, perturbation zonal velocity, meridional velocity and geopotential, respectively. Meridional velocity v is defined to be out of phase with u and ϕ. k and ω ($\equiv \omega_r + \mathrm{i}\omega_i$) are zonal wavenumber and complex frequency, respectively. Linearized perturbation equations are non-dimensionalized by the length scale γ/β, which is the latitudinal width of the inertially unstable region, time scale γ^{-1}, velocity scale γ^2/β, and geopotential scale γ^4/β^2; $\beta \equiv \mathrm{d}f/\mathrm{d}y$ (f is the Coriolis parameter) and $\gamma \equiv \partial\bar{u}/\partial y$. The only non-dimensional parameter is $E \equiv \gamma^4/(gH\beta^2)$, where g and H are gravitational constant and equivalent depth, respectively. The non-dimensional parameter E corresponds to four powers of the ratio of γ/β to equatorial radius of deformation $(gH)^{1/4}/\sqrt{\beta}$.

In this paper, we adopt

$$\bar{u}(y) = y + 2, \tag{2.4}$$

as the basic zonal flow (figure 1). In this basic flow, an inertially unstable region exists in the region of $0 \leqslant y \leqslant 1$. Shear instability does not occur, since the condition of Kuo (1949) is not satisfied.

The calculation domain is $-2 \leqslant y \leqslant 3$ (figure 1). The eigenvalue equations, (2.1) to (2.3), are solved by discretizing in the y-direction with 64 grid points. Supplementary calculations for the cases with a calculation domain of $-3 \leqslant y \leqslant 3$ and $-2 \leqslant y \leqslant 5$, and for the cases with 128 and 512 grid points are also performed. Differences of the

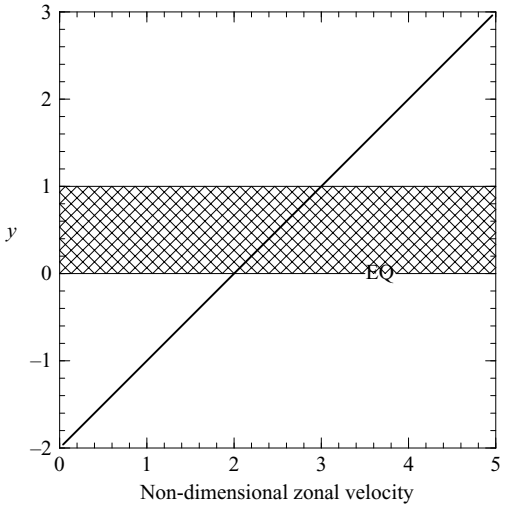

FIGURE 1. Meridional profile of the basic flow: $\overline{u} = y + 2$. Horizontal and vertical axes are velocity and y, respectively. The shaded area indicates the inertially unstable region.

results from those shown in the following sections are not so large that we need to alter our conclusions. The maximum zonal wavenumber is 1, which corresponds to the short-wave cutoff (Boyd & Christidis 1982; Dunkerton 1983). Values of E within the range of $-2.50 \leqslant \log E \leqslant 7.50$ (i.e. $3.16 \times 10^{-3} \leqslant E \leqslant 3.16 \times 10^{7}$) are considered.

3. Numerical results of the eigenvalue problem

Figure 2 shows non-dimensional growth rates ω_i of unstable modes as a function of E and k. Unstable modes appear in the range $\log E \gtrsim -1.00$ in our system. However, as described in the next section, the critical value at which unstable modes appear changes according to the meridional width of the calculation domain. For $-1.00 \lesssim \log E \lesssim 1.20$, only zonally non-symmetric ($k \neq 0$) modes are destabilized. Wavenumbers of the most unstable modes oscillate in the range of $-0.90 \lesssim \log E \lesssim -0.20$ and have a discontinuity at $\log E \sim -0.20$; the reasons for this are discussed in § 5. Symmetric ($k = 0$) unstable modes arise for $\log E \gtrsim 1.20$. This value of $\log E$ corresponds to the critical value, obtained by Stevens (1983), at which symmetric inertially unstable modes appear. For $1.20 \lesssim \log E \lesssim 2.00$, non-symmetric unstable modes dominate symmetric modes, while symmetric unstable modes dominate non-symmetric modes for $\log E \gtrsim 2.00$. The value of $\log E \simeq 2.00$ corresponds to the critical value obtained by Clark & Haynes (1996) at which the fastest growing mode exchanges to non-symmetric modes from symmetric modes.

In the following, we examine the horizontal structure of the most unstable mode for each value of E. Figure 3 shows the horizontal structures of u, v and ϕ and the amplitudes of the terms in equations (2.1) to (2.3) of a typical most unstable mode for a value of $\log E \gtrsim 2.00$. The structure shown in figure 3(a) is equivalent to that of zonally symmetric inertially unstable modes discussed by Stevens (1983): (i) u and v have opposite signs in the unstable region; (ii) amplitudes of u and v have extrema near the *dynamic equator* (the latitude of the centre of the inertially unstable region, Boyd 1978); and (iii) the amplitude of ϕ has extrema on either side of the dynamic equator within the inertially unstable region. The time evolution of u is determined by $v(1 - y)$ (figure 3b). This term causes the growth of u, since $(1 - y)$ is positive

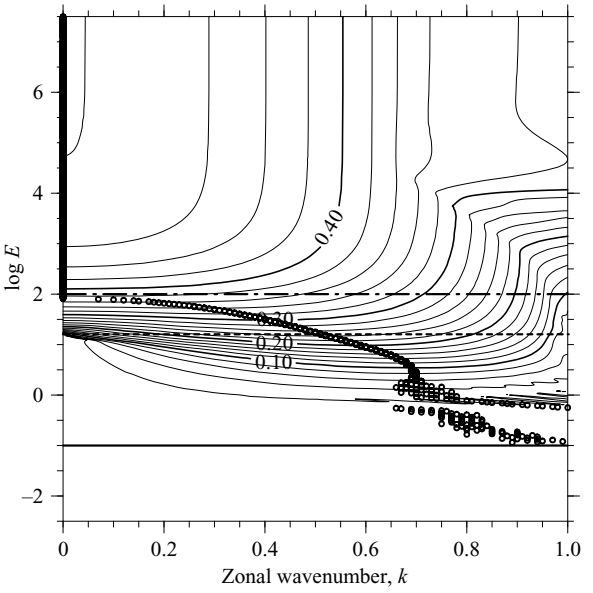

FIGURE 2. Non-dimensional growth rate ω_i as a function of k and E. The most unstable mode for each value of E is indicated by an open circle. The solid line, dotted line, and dash-dotted line indicate, respectively, $\log E = -1.00$ at which non-symmetric unstable modes emerge, $\log E = 1.20$ at which symmetric unstable modes emerge, and $\log E = 2.00$ at which symmetric modes become the most unstable. Contour interval is 2×10^{-2}.

throughout the inertially unstable region and v has the opposite sign to that of u. In figure 3(c), the Coriolis force overcomes the pressure gradient force. The Coriolis term amplifies v, since u has the opposite sign to v. Figure 3(d) shows that the time evolution of ϕ is due to $(1/E)(\partial v/\partial y)$. The structure of v with its large amplitude at the dynamic equator leads to the amplification of $\partial v/\partial y$ on either side of the dynamic equator within the unstable region, and to the growth of ϕ there.

Figure 4 shows one of the most unstable modes in the range $1.20 \lesssim \log E \lesssim 2.00$. This mode corresponds to the non-symmetric unstable modes obtained by Boyd & Christidis (1982) and Dunkerton (1983). For these values of $\log E$, zonally non-symmetric modes are the most unstable. The horizontal structure of the mode (figure 4a, e, i) has similar features to that of $\log E \gtrsim 2.00$: u and v have opposite signs and the amplitudes have extrema near the dynamic equator. The field of ϕ, although deformed by the shear of the basic flow, has an anti-symmetric structure with respect to the dynamic equator, and the structure is similar to that of the westward mixed Rossby–gravity wave shown by Matsuno (1966). The time evolution of the mode is also similar to that of $\log E \gtrsim 2.00$ in which symmetric modes are dominant: the growth of u and v are caused by the dominance of the Coriolis term and the opposite signs of u and v (figure 4a–h), and the growth of ϕ is caused mainly by $(1/E)\partial v/\partial y$ (figure 4i–l).

Figure 5 shows one of the most unstable modes in the range $-1.00 \lesssim \log E \lesssim 1.20$. This corresponds to the small shear case discussed by Boyd & Christidis (1982). Contrary to the modes seen so far, there exists a region in which u and v have the same sign, and extrema of the amplitudes exist outside the inertially unstable region. The phase relationship between ϕ and u, v is similar to that of the eastward equatorial Kelvin wave. The growing mechanism of the mode is different from those

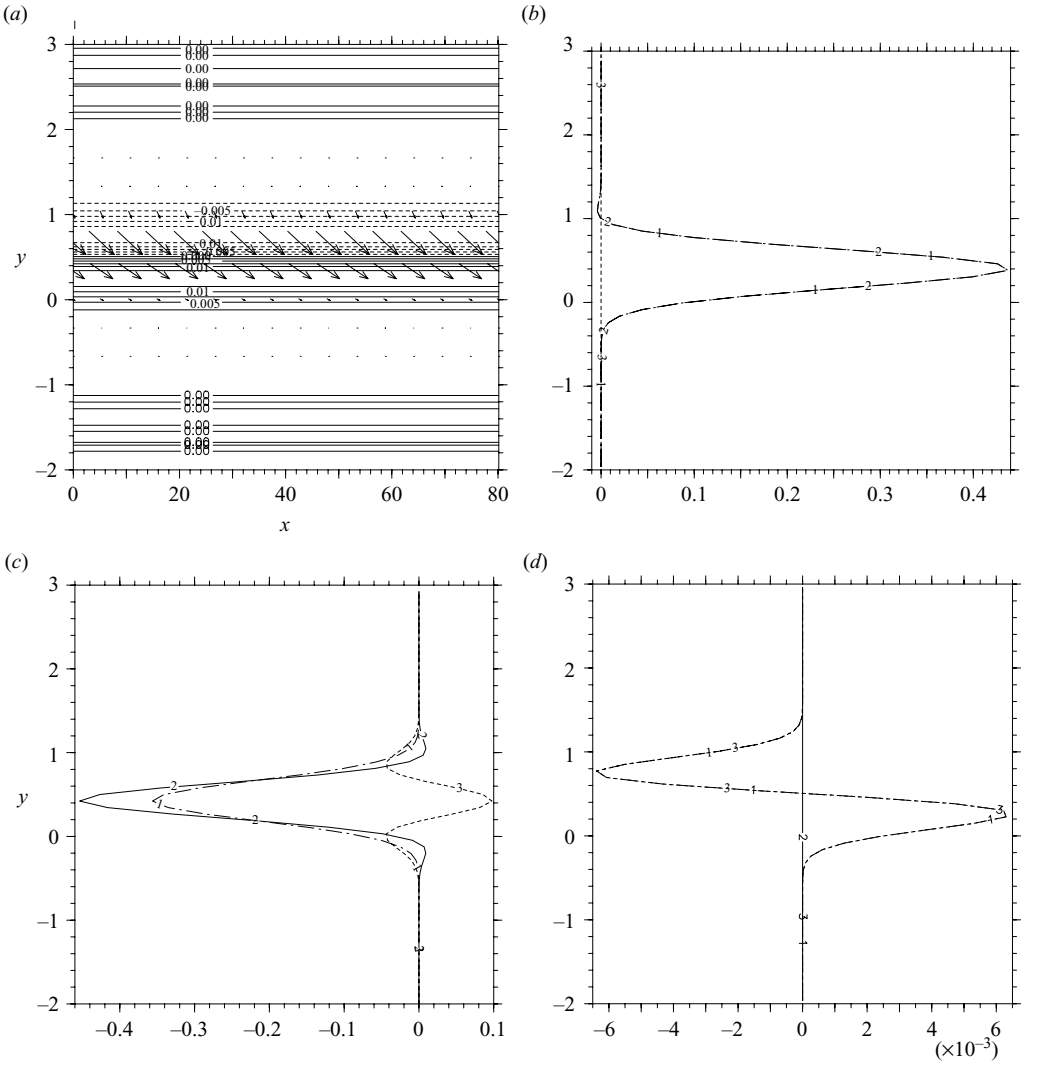

FIGURE 3. Horizontal structure of the most unstable mode with $\log E = 2.50, k = 0$. (*a*) Horizontal structure of velocity (vectors) and geopotential ϕ (contours). Contour intervals are 0.0025. Dashed contours correspond to negative values. (*b*) Magnitudes of the terms in equation (2.1) at $x = 0$. Lines with indices '1', '2' and '3' indicate $-(\omega - k\bar{u})u$, $-v(1 - y)$ and $-k\phi$, respectively. (*c*) Magnitudes of the terms in equation (2.2) at $x = 0$. Lines with indices '1', '2' and '3' indicate $(\omega - k\bar{u})v$, $-yu$ and $-\partial\phi/\partial y$, respectively. (*d*) Magnitudes of the terms in equation (2.3) at $x = 0$. Lines with indices '1', '2' and '3' indicate $-(\omega - k\bar{u})\phi$, $-ku/E$ and $-(1/E)\partial v/\partial y$, respectively. In (*b*) and (*d*), the real part of each term multiplied by $\mathrm{i}e^{\mathrm{i}kx}$ is plotted. In (*c*), the real part of each term multiplied by $e^{\mathrm{i}kx}$ is plotted.

of the most unstable modes for $\log E \gtrsim 2.00$ in which symmetric modes are dominant, and for $1.20 \lesssim \log E \lesssim 2.00$ in which non-symmetric modes are dominant. The growth of u and v depends on the pressure gradient term as well as on the Coriolis term (figures 5*a–d* and 5*e–h*). Both $(1/E)(ku)$ and $(1/E)(\partial v/\partial y)$ in equation (2.3) lead to the development of ϕ (figure 5*i–l*). All the most unstable modes for $-1.00 \lesssim \log E \lesssim 1.20$ show a similar structure to figure 5 near the equator, although the structure of the

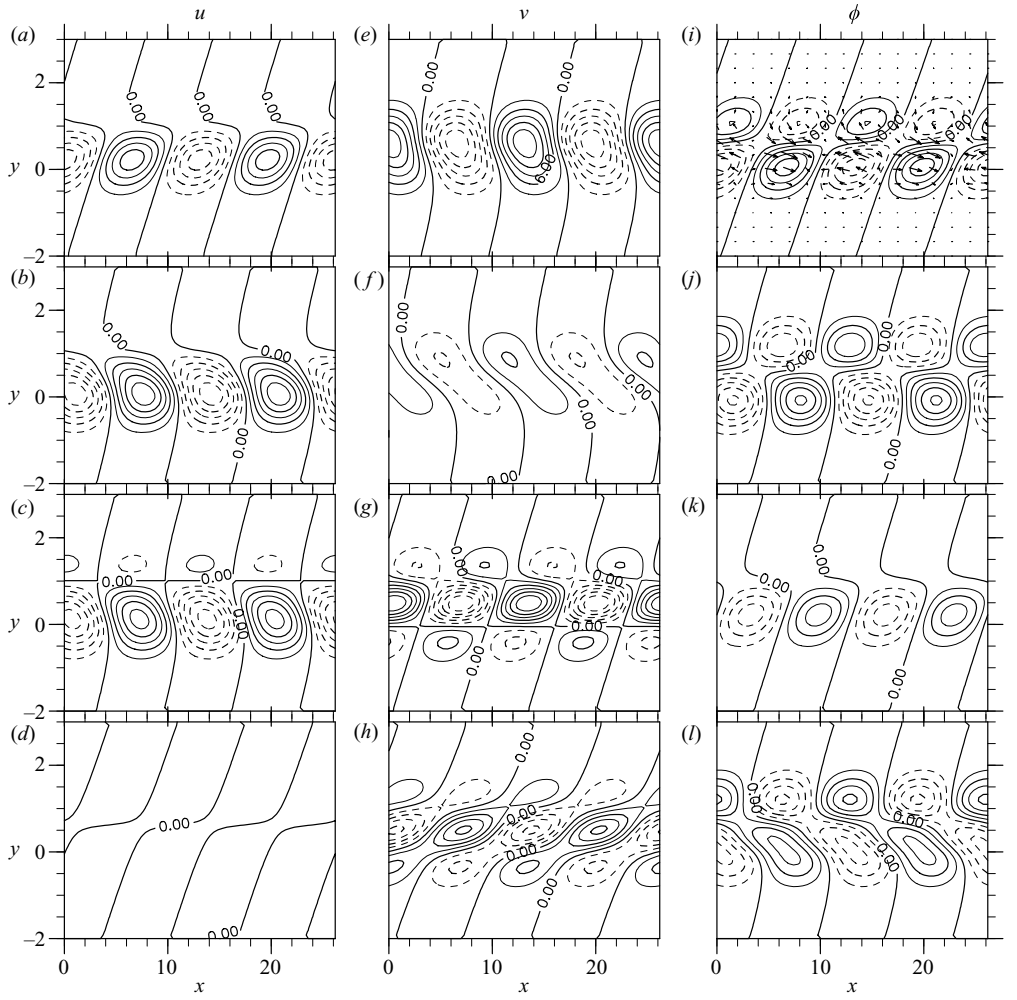

FIGURE 4. Horizontal structure of the real part of terms in equations (2.1) to (2.3) for the most unstable mode with $\log E = +1.30$, $k = 0.48$. (*a*) u, (*b*) $-(\omega - k\bar{u})u$, (*c*) $-v(1-y)$, (*d*) $-k\phi$, (*e*) v, (*f*) $(\omega - k\bar{u})v$, (*g*) $-yu$, (*h*) $-\partial\phi/\partial y$, (*i*) ϕ and velocity vector (u, v), (*j*) $-(\omega - k\bar{u})\phi$, (*k*) $-(ku/E)$ and (*l*) $-(1/E)(\partial v/\partial y)$. In (*b*)–(*d*) and (*j*)–(*l*), the real part of each term multiplied by ie^{ikx} is plotted. In (*f*)–(*h*), the real part of each term multiplied by e^{ikx} is plotted. Contour intervals are 8.00 in (*a*), 2.00 in (*b*)–(*d*), 3.00 in (*e*), 2.50 in (*f*)–(*h*), 0.80 in (*i*), and 0.25 in (*j*)–(*l*). Dashed contours correspond to negative values.

boundary Kelvin wave emerges near the north boundary for $\log E \sim 0$ (figures not shown).

4. Characteristics of dispersion curves

In this section, we examine intersections of dispersion curves and the signs of the pseudomomenta of modes according to the resonance between neutral waves. Figure 6(*a*) shows dispersion curves for $\log E = -1.10$ in which no unstable mode exists. Continuous modes exist with c in the range of $\bar{u}$, i.e. $0 \leqslant c \leqslant 5$, and the discretized versions of these modes can be seen in this figure. The modes with phase speed ($c \approx 6.0$ at $k = 0$) larger than continuous modes are equatorial Kelvin

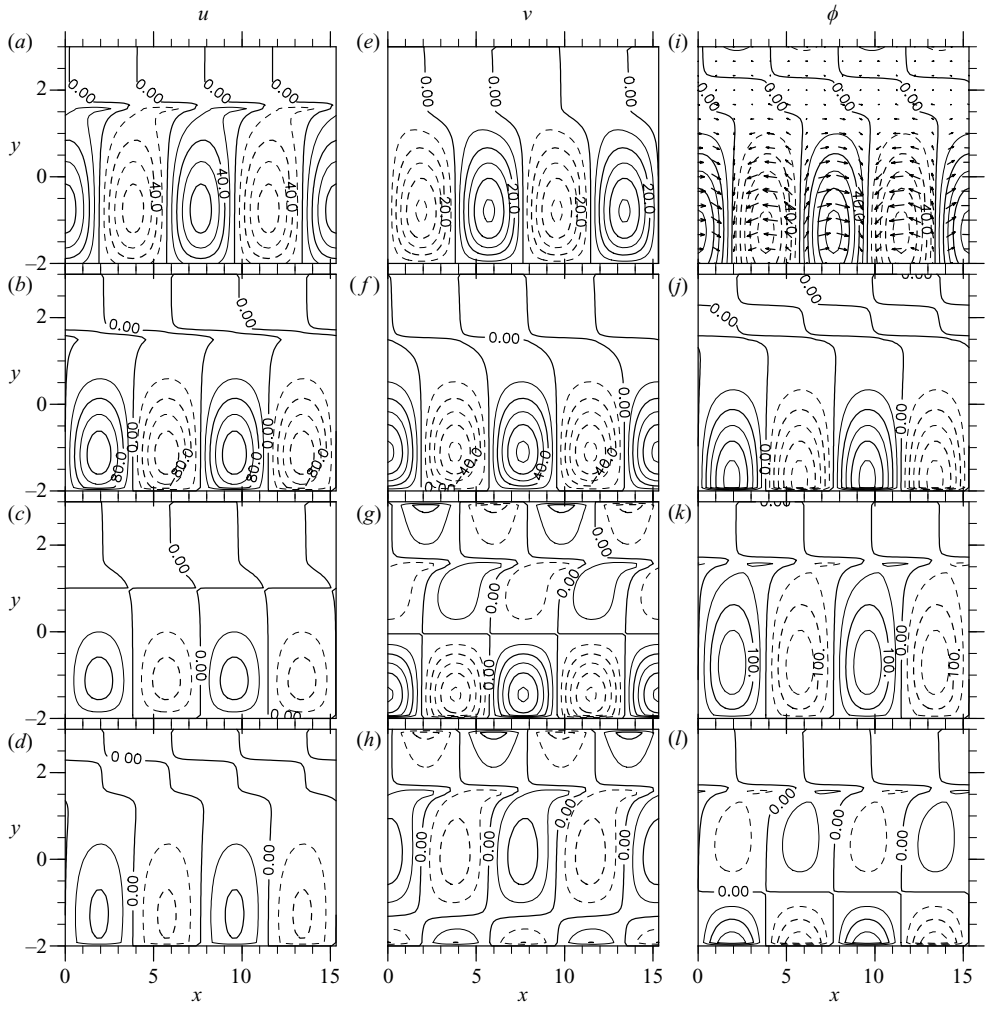

FIGURE 5. Same as figure 4, but for $\log E = -0.40$, $k = 0.82$. Contour intervals are 20.0 in (a), 40.0 in (b)–(d), 10.0 in (e), 20.0 in (f)–(h), 20.0 in (i), and 50.0 in (j)–(l).

modes. The modes with phase speed smaller than continuous modes are westward mixed Rossby–gravity modes. These neutral modes can be identified by examining their structures for the case where the dispersion curves do not intersect those of continuous modes (figures not shown). In figure 6(a), the boundary Kelvin wave near the north boundary cannot be recognized, since it assimilates into continuous modes. For smaller E (figures not shown), its phase speed has a smaller value than those of continuous modes and the dispersion curves can be observed.

All of the modes in figure 6(a), except for equatorial Kelvin modes, have negative pseudomomenta as described below and, therefore, the intersection of dispersion curves does not generate unstable modes. The sign of pseudomomenta of continuous modes is negative, since continuous modes have pseudomomenta with opposite sign to the gradient of the potential vorticity of basic flow (Iga 1999a). Pseudomomenta of westward mixed Rossby–gravity modes are also negative because pseudomomenta of neutral modes have opposite signs to the gradient of their dispersion curves (Iga

1999*b*). The pseudomomentum of the north boundary Kelvin mode that assimilates into continuous modes is estimated to be negative as follows. If continuous modes did not exist, the dispersion curve of the north boundary Kelvin mode would have zero gradient; therefore, its pseudomomentum M could be calculated by equation (4.1) (Iga 1999*b*):

$$M \sim \tfrac{1}{2} \int \{c - \overline{u}(y)\} |u(y)|^2 \, \mathrm{d}y. \tag{4.1}$$

From this equation, the pseudomomentum of the north boundary Kelvin mode is negative. We speculate that the sign of the pseudomomentum of the north boundary Kelvin mode assimilating into continuous modes remains negative.

As mentioned above, no unstable mode exists for $\log E \lesssim -1.00$ in our configuration. However, this result is not generally robust. With a wider calculation domain, intersection of dispersion curves of equatorial Kelvin modes and continuous modes occurs even for $\log E \lesssim -1.00$, since continuous modes with larger phase speeds emerge (figures not shown). If the calculation domain were infinite, intersection of dispersion curves of equatorial Kelvin modes and continuous modes would occur for any value of E. This is consistent with the previous result that the equatorial Kelvin wave is always destabilized in cross-equatorial shear flow (Natarov & Boyd 2001).

Figure 6(*b*) shows dispersion curves for $\log E = -0.90$ in which only non-symmetric modes are destabilized. In this figure, unstable modes appear where dispersion curves of neutral modes and continuous modes intersect. The horizontal structures of modes leading to the unstable modes are shown in figure 7. The neutral modes leading to the unstable modes (figure 7*a*) can be considered as an eastward equatorial Kelvin wave in shear flow (Boyd 1978), since (i) local extrema of amplitude of ϕ exist at the equator; (ii) ϕ and velocity have symmetric structures with respect to the equator; (iii) $|u| \gg |v|$; and (iv) u and ϕ have the same phase. Other neutral modes with larger wavenumber on the same dispersion curve also have the structure of the equatorial Kelvin wave, although the structures are somewhat distorted (figure not shown). The resonating counterpart is the superposition of continuous modes, such as the critical-layer instability problem discussed by Iga (1999*a*). One of the continuous modes is shown in figure 7(*b*). Therefore, the unstable modes are caused by resonance between equatorial Kelvin modes with positive pseudomomentum and continuous modes with negative pseudomomentum, and correspond to the unstable Kelvin wave discussed by Boyd & Christidis (1982).

In the cases of $\log E = -0.40$, 0.30 and 1.00 (figures 6*c*, 6*d* and 6*e*, respectively), the dispersion curves of the most unstable modes are buried among continuous modes for all k. Therefore, we cannot identify resonating neutral waves only by these figures. However, by observing dispersion curves from $\log E = -0.90$ to $\log E = 1.00$, we can see that the most unstable modes are also caused by the resonance between equatorial Kelvin modes and continuous modes. This is confirmed in § 5. In figures 6(*c*)–6(*f*), other kinds of instabilities can be observed: resonating counterparts of continuous modes are eastward mixed Rossby–gravity modes or eastward inertial gravity modes. (Intersections of dispersion curves of westward mixed Rossby–gravity modes and westward inertial gravity modes with those of continuous modes do not cause instability, since pseudomomenta of these neutral modes are negative and have the same sign as those of continuous modes.) In these figures, dispersion curves of south boundary Kelvin modes can be observed. They consist of the parts of several curves around $c = -1.20$ in figure 6(*c*), around $c = -0.60$ in figure 6(*d*), and

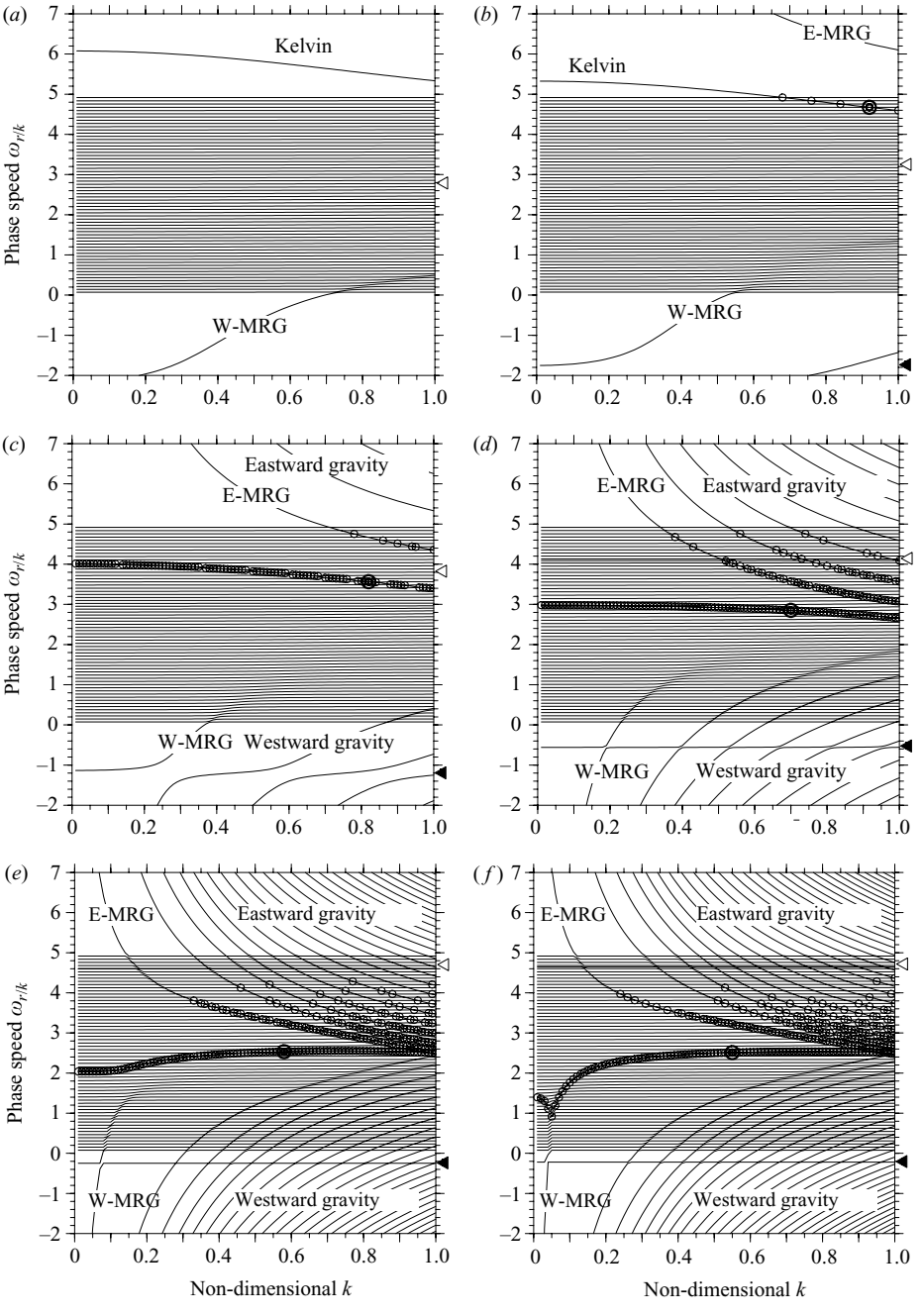

FIGURE 6(a–f). For caption see facing page.

around $c = -0.20$ in figure 6(e). South boundary Kelvin modes do not resonate with westward mixed Rossby–gravity modes or westward inertial gravity modes, since all of the modes have negative pseudomomenta.

While the most unstable modes for $\log E \lesssim 1.00$ are caused by resonance between equatorial Kelvin modes and continuous modes, the most unstable modes for

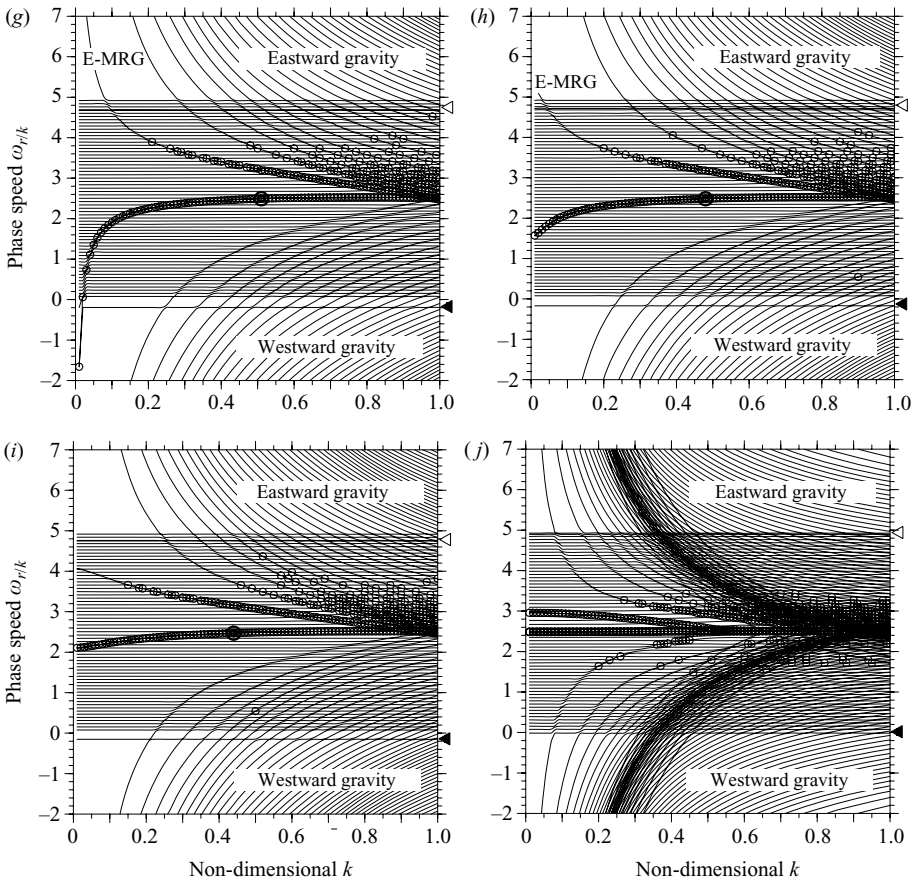

FIGURE 6. Dispersion curves of neutral and unstable modes. Values of $\log E$ are (*a*) −1.10, (*b*) −0.90, (*c*) −0.40, (*d*) +0.30, (*e*) +1.00, (*f*) +1.10, (*g*) +1.20, (*h*) +1.30, (*i*) +1.40 and (*j*) +2.50. Single and double open circles indicate unstable modes and the most unstable modes, respectively. In (*j*), the most unstable mode with $k = 0$ is not shown. Open and filled triangles indicate the positions of dispersion curves of north and south boundary Kelvin modes, respectively. The labels 'E-MRG' and 'W-MRG' indicate eastward mixed Rossby–gravity modes and westward mixed Rossby–gravity modes, respectively.

$\log E \gtrsim 1.00$ are caused by another type of resonance. One of resonating neutral modes is westward mixed Rossby–gravity modes, which can be observed in figures 6(*e*) and 6(*f*). The structure of the mode is shown in figure 8. It has characteristics similar to that of figure 6(*b*) of Matsuno (1966). The resonating counterparts of westward mixed Rossby–gravity modes cannot be identified by examining only figures 6(*e*)–6(*g*). For $\log E = 1.30$, 1.40 and 2.50 (figures 6*h*, 6*i* and 6*j*, respectively), the dispersion curves of the most unstable modes are buried among continuous modes, and neutral modes leading to instability cannot be identified. The resonating neutral modes in these cases are identified in § 6.

Phase speed of the most unstable mode approach basic flow velocity at dynamic equator, $\overline{u}(y = 0.5) = 2.5$, in the limit of large E (figure 6*j*). This result is consistent with that of asymptotic expansion by Clark & Haynes (1996). It is also confirmed that the same result is obtained for the case with a calculation domain which is not symmetric with respect to the dynamic equator ($-3 \leqslant y \leqslant 3$).

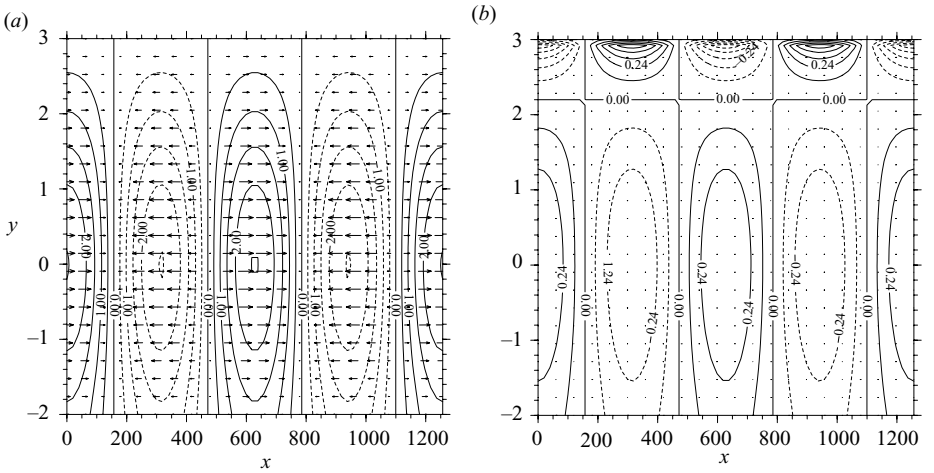

FIGURE 7. Horizontal structures of modes leading to the most unstable modes for $\log E = -0.90$. (*a*) Equatorial Kelvin mode with $k = 0.01, c \simeq 5.30$, (*b*) continuous modes with $k = 0.01, c \simeq 4.90$. Contours and vectors indicate ϕ and the velocity field, respectively. Contour intervals are (*a*) 0.50, (*b*) 0.12. Dashed contours correspond to negative values.

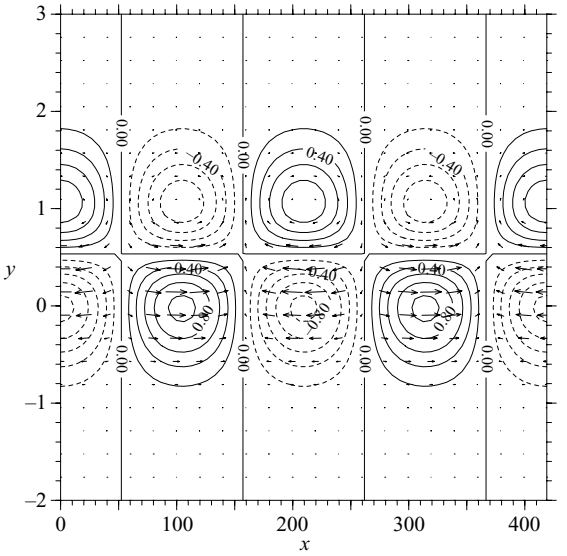

FIGURE 8. Horizontal structure of westward mixed Rossby–gravity mode for $\log E = +1.10$, $k = 0.03$. Contours and vectors indicate ϕ and the velocity field, respectively. Contour interval is 0.20. Dashed contours correspond to negative values.

5. Identification of equatorial Kelvin modes

As mentioned in §4, neutral waves leading to instability cannot be extracted for larger values of E since the dispersion curves are buried in those of continuous modes. In this section, we use other methods to identify the dispersion curves of equatorial Kelvin modes buried in continuous modes. First, we apply two approximations in order to derive analytically an approximate dispersion relation of equatorial Kelvin modes for small k. Secondly, we perform numerical calculations for basic flows which

have a uniform velocity region to extract the dispersion curves of equatorial Kelvin modes.

5.1. *The approximate dispersion relation of equatorial Kelvin modes*

In this subsection, we derive the approximate formula of a dispersion relation of equatorial Kelvin modes using two approximations and extract equatorial Kelvin modes from continuous modes. First, we assume that

$$\omega - k\overline{u}(y) \simeq \omega - k\tilde{u} \equiv \hat{\omega}, \tag{5.1}$$

where $\tilde{u}$ is a constant value and is set to be the velocity of the basic flow at the dynamic equator, 2.5. This assumption is consistent with the result of asymptotic expansion by Clark & Haynes (1996) in the limit of large E. Moreover, we assume that the horizontal structure of the equatorial Kelvin wave in a shear flow is similar to that in non-shear flow, and set v to be zero. Strictly speaking, the meridional velocity v of an equatorial Kelvin wave in shear flow is not zero (Boyd 1978). However, equatorial Kelvin modes obtained in § 3 have the characteristic of $u \gg v$ for small wavenumber. With the above assumptions, equations (2.1) to (2.3) are rewritten as follows:

$$-\hat{\omega}u = -k\phi, \tag{5.2}$$

$$yu = -\frac{\partial \phi}{\partial y}, \tag{5.3}$$

$$-\hat{\omega}\phi = -k\frac{1}{E}u. \tag{5.4}$$

From equations (5.2) to (5.4), the phase speed is given as

$$c = \tilde{u} + \frac{1}{\sqrt{E}}. \tag{5.5}$$

Figure 9 shows the approximate dispersion curve given by equation (5.5) and the numerically obtained dispersion curves which have been given in § 4. For the case of $\log E = -1.10$ (figure 9*a*), equatorial Kelvin modes can be identified with numerical results, since their dispersion curve exists above those of continuous modes. The approximate dispersion curve (blue line in figure 9*a*) coincides well with the numerically obtained dispersion curve for $0 < k \leqslant 0.20$. Therefore, it is expected that the dispersion curves of equatorial Kelvin modes in the small k range can also be estimated for the cases where the dispersion curves are buried among continuous modes. For $\log E = -0.40$ (figure 9*b*), the dispersion curve of the most unstable modes is in good agreement with the approximate dispersion curve in the small k range. Consequently, the most unstable modes can be considered to be caused by resonance between equatorial Kelvin modes and continuous modes and to be identical with the destabilized Kelvin waves discussed by Boyd & Christidis (1982).

However, for $\log E = 1.00$ (figure 9*c*), the approximate phase speed of equatorial Kelvin modes deviates from those of the most unstable modes obtained by numerical calculation. The reason for the deviation for larger values of E has not been fully examined. We speculate that the existence of westward mixed Rossby–gravity modes causes the deviation since, as shown in figure 13, the deviation occurs only in the neighbourhood of $\log E = 1.00$ at which resonating mixed Rossby–gravity modes emerge. The above results are also obtained for the cases with the domains of $-3 \leqslant y \leqslant 3$ and of $-2 \leqslant y \leqslant 5$ (figure not shown). In the next subsection, we directly

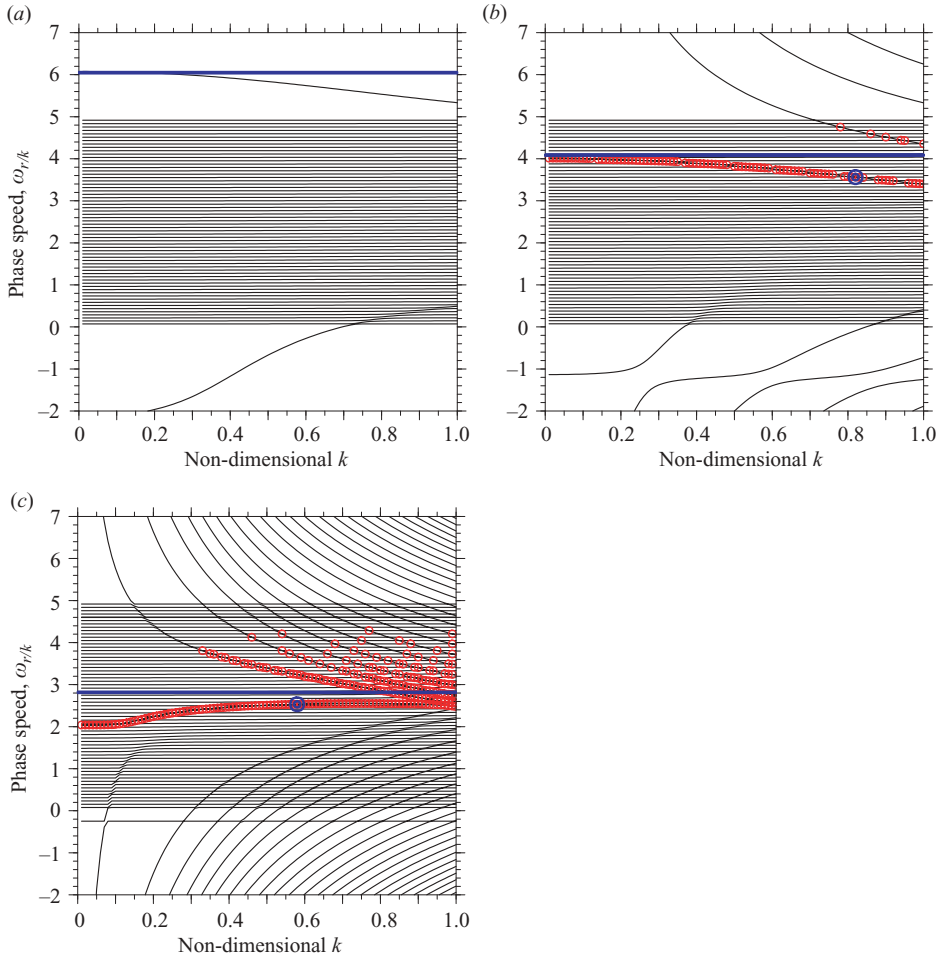

FIGURE 9. Approximate dispersion curves of equatorial Kelvin wave modes (blue line) obtained by equation (5.5) and numerically obtained dispersion curves. Values of $\log E$ are (*a*) −1.10, (*b*) −0.40, and (*c*) +1.00. Single red circles and double blue circles indicate unstable modes and the most unstable modes obtained by numerical calculation in § 4, respectively.

extract the dispersion curves of equatorial Kelvin modes buried among the dispersion curves of continuous modes.

5.2. *Eigenvalue problem for basic flows with a uniform velocity region*

In this subsection, we solve eigenvalue problems where part of the basic flow is distorted and extract equatorial Kelvin modes from continuous modes into which equatorial Kelvin modes assimilate. On the basis of a theorem of Lin (1945), Iga (1999*c*) succeeded in extracting the neutral waves buried among continuous modes by considering basic flows having a uniform potential vorticity region. However, the approach used by Iga (1999*c*) for shallow water on an f-plane is not suitable for our system since the equatorial neutral waves are eliminated in basic states with a uniform potential vorticity region. In this paper, the basic states with a uniform velocity region are considered. In a uniform velocity region, continuous modes are expected to be excluded and neutral modes can be extracted since phase speed of continuous modes

is equal to basic state velocity at each discretized grid point. The equatorial waves do not disappear in this case, since the β-effect remains in the basic state.

Three kinds of basic flow are considered so as to extract neutral modes around the dispersion curves of the most unstable modes: $\bar{u}$ with a uniform velocity region in $1.40 \leqslant y \leqslant 2.00$ for $\log E = -0.40$ (figure 10*a*); $\bar{u}$ with a uniform velocity region in $0.40 \leqslant y \leqslant 1.00$ for $\log E = 0.30$ (figure 10*c*); and $\bar{u}$ with a uniform velocity region in $-0.30 \leqslant y \leqslant 0.30$ for $\log E = 1.30$ (figure 10*e*). With these basic flows, continuous modes are successfully eliminated in the regions of $3.40 \leqslant c \leqslant 4.00$ for $\log E = -0.40$ (figure 10*b*), $2.40 \leqslant c \leqslant 3.00$ for $\log E = 0.30$ (figure 10*d*), and $1.60 \leqslant c \leqslant 2.20$ for $\log E = 1.30$ (figure 10*f*). For $\log E = -0.40$ and $\log E = 0.30$, additional unstable modes emerge at $c \approx 3.70$ in figure 10(*b*) and at $c \approx 2.70$ in figure 10(*d*) because of the existence of the inflection points of the basic flow. Besides additional unstable modes, neutral modes can be observed in the region in which no continuous mode exists. In figure 10(*b*), dispersion curves of neutral modes exist around $0.20 \leqslant k \leqslant 0.50$ and $3.80 \leqslant c \leqslant 4.00$, and around $0.80 \leqslant k \leqslant 0.95$ and $3.40 \leqslant c \leqslant 3.60$. The neutral modes of figure 10(*d*) appear in the region of $0.65 \leqslant k \leqslant 0.85$ and $2.60 \leqslant c \leqslant 3.00$. The horizontal structure of the neutral mode is shown in figure 11. Although the structure is somewhat distorted compared with figure 7(*a*), it has the characteristics of equatorial Kelvin modes. For other cases with $\log E \lesssim 1.00$ in which only non-symmetric modes are destabilized, it turns out that dispersion curves of the most unstable modes coincide with dispersion curves of equatorial Kelvin modes for basic flows with uniform velocity regions (figures not shown). Therefore, it is considered that the most unstable modes in $\log E \lesssim 1.00$ are caused by resonance between equatorial Kelvin modes and continuous modes.

However, for $\log E \gtrsim 1.00$, neutral modes do not appear in uniform velocity regions. In figure 10(*f*), neutral modes do not appear, but unstable modes remain in the region of $1.60 \leqslant c \leqslant 2.20$ in which no continuous mode exists. The dispersion curve of the unstable modes is similar to the dispersion curve of the most unstable modes in figure 6(*h*). In contrast to the cases of $\log E \lesssim 1.00$, neutral modes cannot be found with basic flows with uniform velocity regions when $\log E \gtrsim 1.00$. The reason for this is that the most unstable modes in these cases are caused by resonance between two neutral modes; therefore, unstable modes exist even though continuous modes are excluded. The resonating neutral waves for $\log E \gtrsim 1.00$ are discussed in the next section.

The result that the most unstable modes for $\log E \lesssim 1.00$ are caused by resonance between equatorial Kelvin modes and continuous modes explains the curious distribution of the most unstable modes in figure 2. The discontinuity of the most unstable modes at $\log E \sim -0.20$ is caused by the change of the property of continuous modes. For $\log E \sim -0.20$, the north boundary Kelvin wave assimilates into continuous modes which resonate with equatorial Kelvin modes (figures not shown). Such discontinuity does not emerge in the case with the wider calculation domain of $-2 \leqslant y \leqslant 5$. In figure 2, it can be seen also that wavenumbers of the most unstable modes oscillate in the range $-0.90 \lesssim \log E \lesssim -0.20$. The oscillation is caused by the change of combination of continuous modes resonating with equatorial Kelvin modes whose phase speeds decrease according to the increase of E. In figure 2, which is obtained with 64 grid points in the y-direction, the change of combination of continuous modes is emphasized, since the interval of the neighbouring continuous mode is not small enough. Supplementary calculations with 128 grid points in the y-direction show a smoother distribution of the most unstable modes in the range $-0.90 \lesssim \log E \lesssim -0.20$ (figure not shown).

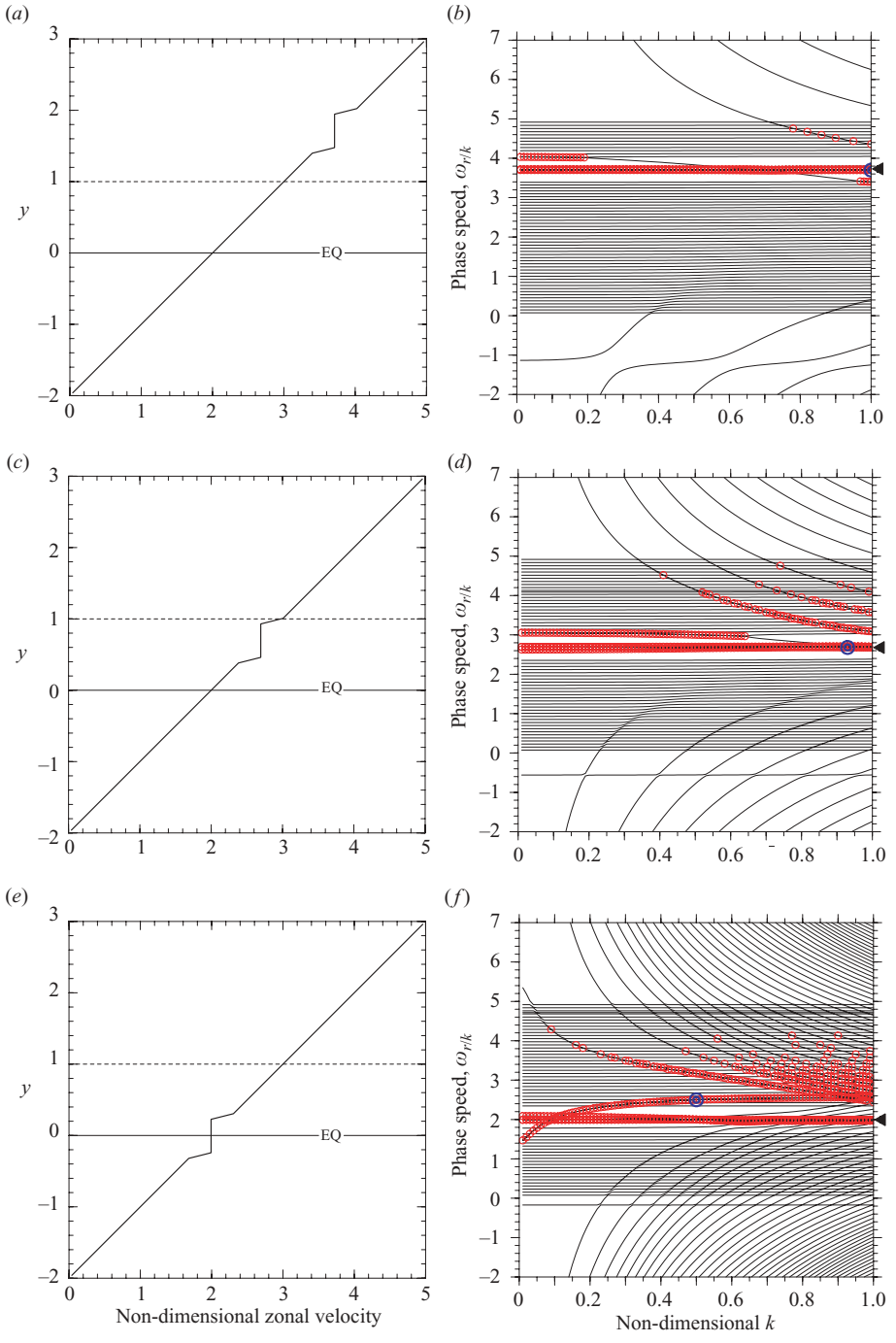

FIGURE 10. Basic flows with uniform velocity regions (*a*), (*c*), (*e*), and the resulting dispersion curves (*b*), (*d*), (*f*). The values of $\log E$ are -0.40 for (*a*) and (*b*), $+0.30$ for (*c*) and (*d*), and $+1.30$ for (*e*) and (*f*). Single red circles and double blue circles in (*b*), (*d*), and (*f*) indicate unstable modes and the most unstable modes, respectively. Filled triangles indicate the positions of the dispersion curves of additional unstable modes owing to inflection points introduced by uniform velocity regions.

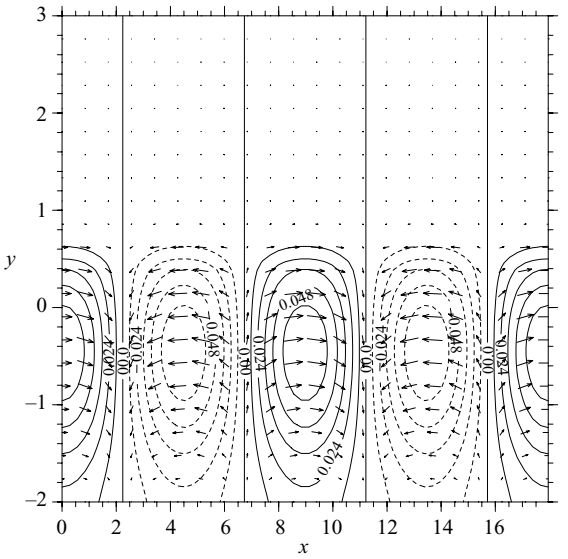

FIGURE 11. Horizontal structure of the neutral mode with $\log E = 0.30$ and $k = 0.70$ for the basic flow shown in figure 10(*c*). Contours and vectors indicate ϕ and the velocity field, respectively. Contour interval is 0.012. Dashed contours correspond to negative values.

6. Identification of mixed Rossby–gravity modes

In this section, we clarify the resonating neutral waves in the neighbourhood of $\log E = 1.20$ by the use of the 'uniform Γ-plane' approximation (Boyd & Christidis 1982) which gives the approximate formula of the dispersion relations of modes of a linear shear flow in shallow water on an equatorial β-plane. After reducing equations (2.1) to (2.3) down to one for v alone, by assuming that

$$\omega - k\bar{u}(y) \simeq \omega - k\tilde{u} \equiv \hat{\omega}, \quad \tilde{u} = 2.5, \tag{6.1}$$

as in § 5.1, terms with order up to $O[(k/\hat{\omega})^1]$ in the equation yield

$$\frac{\partial^2 v}{\partial y^2} + \left[-\frac{k}{\hat{\omega}} - E\{y(y-1) - \hat{\omega}^2\}\right] v = 0. \tag{6.2}$$

Except for the definition of $\hat{\omega}$, equation (6.2) is equivalent to equation (12) of Boyd & Christidis (1982). Equation (6.2) does not have singular points, and continuous modes are excluded. Because equation (6.2) can be transformed into Schrödinger's equation for the harmonic oscillator, the dispersion relation is obtained as

$$\hat{\omega}^3 + \left\{\tfrac{1}{4} - \frac{1}{\sqrt{E}}(2n+1)\right\}\hat{\omega} - \frac{k}{E} = 0 \qquad (n = 0, 1, 2, \ldots). \tag{6.3}$$

With

$$Q \equiv \frac{1}{3}\left(\frac{2n+1}{\sqrt{E}} - \frac{1}{4}\right), \tag{6.4}$$

$$R \equiv -\frac{k}{2E}, \tag{6.5}$$

$$S \equiv (\sqrt{R^2 - Q^3} + |R|)^{1/3}, \tag{6.6}$$

$$\theta \equiv \arccos\left(\frac{R}{\sqrt{Q^3}}\right), \tag{6.7}$$

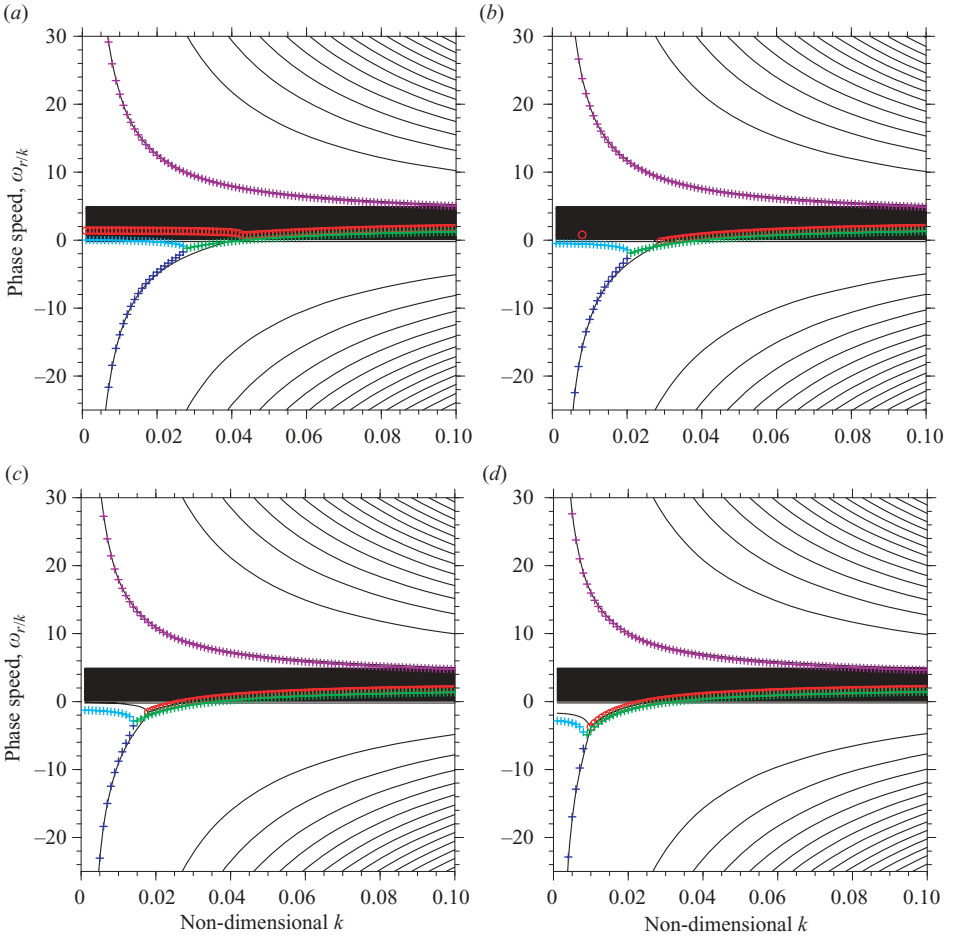

FIGURE 12(*a–d*). For caption see facing page.

the solutions of (6.3) are expressed as follows: for $Q^3 - R^2 \geqslant 0$,

$$\hat{\omega}_1 = -2\sqrt{Q}\cos\frac{\theta}{3}, \tag{6.8}$$

$$\hat{\omega}_2 = -2\sqrt{Q}\cos\frac{\theta + 2\pi}{3}, \tag{6.9}$$

$$\hat{\omega}_3 = -2\sqrt{Q}\cos\frac{\theta + 4\pi}{3}, \tag{6.10}$$

and for $Q^3 - R^2 < 0$,

$$\hat{\omega}_1 = S + \frac{Q}{S}, \tag{6.11}$$

$$\hat{\omega}_2 = -\frac{1}{2}\left(S + \frac{Q}{S}\right) + \mathrm{i}\frac{\sqrt{3}}{2}\left(S - \frac{Q}{S}\right), \tag{6.12}$$

$$\hat{\omega}_3 = -\frac{1}{2}\left(S + \frac{Q}{S}\right) - \mathrm{i}\frac{\sqrt{3}}{2}\left(S - \frac{Q}{S}\right). \tag{6.13}$$

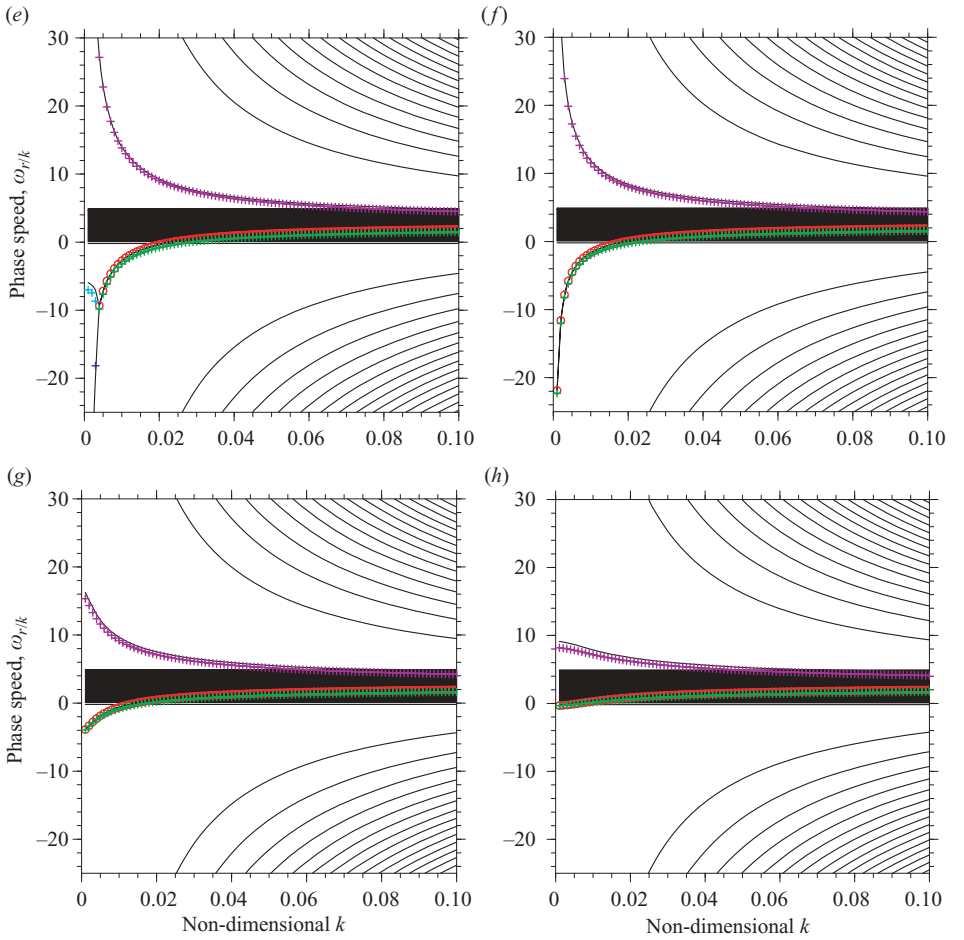

FIGURE 12. Approximate dispersion curves obtained from equations (6.8) to (6.12) for $n=0$. Horizontal and vertical axes are k and c, respectively. The range $0<k\leqslant 0.10$ is shown. The values of $\log E$ are (*a*) +1.10, (*b*) +1.12, (*c*) +1.14, (*d*) +1.16, (*e*) +1.18, (*f*) +1.20, (*g*) +1.22 and (*h*) +1.24. The light blue lines, dark blue lines, and green lines indicate the dispersion curves expressed by equation (6.10) (Kelvin modes), equation (6.8) (westward mixed Rossby–gravity modes), and equation (6.12) (unstable modes), respectively. The purple lines indicate the dispersion curves expressed by equations (6.9) and (6.11) (eastward mixed Rossby–gravity modes). Single red circles indicate unstable modes obtained by the numerical calculation in § 4.

The types and the stability of modes change at k which gives $Q^3-R^2=0$; $k=0$ for $\log E=1.20$, $k\simeq 0.066$ for $\log E=1.00$, and $k\simeq 0.10$ for $\log E=0.90$, where $n=0$. $Q^3-R^2\geqslant 0$ corresponds to the case of small k, if E and n are fixed. In this case, eigen-solutions are three neutral modes. $Q^3-R^2<0$ corresponds to the case of large k. In this case, eigen-solutions consist of neutral modes with $\hat{\omega}_1$, unstable modes with $\hat{\omega}_2$, and decaying modes with $\hat{\omega}_3$. The phase speed of each mode is expressed as $c=\mathrm{Re}(\hat{\omega})/k+\tilde{u}$.

Figure 12 shows the approximate dispersion curves of $n=0$ modes given by equations (6.8) to (6.12) and the numerical results obtained with equations (2.1) to (2.3) in the neighbourhood of $\log E=1.20$. For $1.10\leqslant\log E\leqslant 1.18$ (figure 12*a–e*), approximate solutions consist of three neutral modes (purple lines, light blue lines,

dark blue lines) in the small k region, and of neutral modes (purple lines), unstable modes (green lines), and decaying modes (figures not shown) in the large k region. The three neutral modes in the small k region are identified as follows: purple lines are eastward mixed Rossby–gravity modes, light blue lines are equatorial Kelvin modes, and dark blue lines are westward mixed Rossby–gravity modes. The neutral modes for large k are eastward mixed Rossby–gravity modes. The identifications of the neutral modes mentioned above are based on the correspondence of the approximate dispersion curves obtained by equations (6.8) to (6.13) to the numerically obtained solutions that were identified in previous sections. The dispersion curve of the equatorial Kelvin mode (light blue lines) is distorted and the phase speed becomes negative for $1.10 < \log E < 1.20$ (figure 12*a–e*). This is discussed in the last paragraph of this section.

The numerically obtained unstable modes for $\log E = 1.10$ (figure 12*a*) are interpreted as follows. For small k, near the dispersion curve of the unstable modes obtained by numerical calculation, only the dispersion curve of equatorial Kelvin modes (light blue line) exists. The dispersion curve of westward mixed Rossby–gravity modes (dark blue line) exists away from the dispersion curves of the most unstable modes. These do not suggest that unstable modes obtained by numerical calculation are caused by resonance between two neutral waves. It can be considered that numerically obtained unstable modes are caused by resonance between equatorial Kelvin modes and continuous modes since continuous modes are excluded in equation (6.2). On the other hand, for large k, unstable modes (green line) emerge at the points of intersection of the approximate dispersion curves of equatorial Kelvin modes (light blue line) and westward mixed Rossby–gravity modes (dark blue line). The dispersion curve of the numerically obtained unstable modes (red line) coincides with the approximate dispersion curve of unstable modes, hence, unstable modes for large k can be considered to be caused by the resonance between equatorial Kelvin modes and westward mixed Rossby–gravity modes. The results above show that two types of resonance coexist on the dispersion curves of the most unstable modes. (Coexistence of resonance types on the dispersion curves of the most unstable modes occurs for $1.00 \lesssim \log E \lesssim 1.20$, which is suggested by figures similar to figure 13 except for the large k case (figures not shown).) The resonance type of the most unstable mode changes at $\log E \sim 1.00$ for non-small k values; the most unstable modes are caused by resonance between equatorial Kelvin modes and continuous modes for $\log E \lesssim 1.00$ and by resonance between equatorial Kelvin modes and westward mixed Rossby–gravity modes for $\log E \gtrsim 1.00$.

As the value of E increases, unstable modes caused by resonance between equatorial Kelvin modes and westward mixed Rossby–gravity modes appear at smaller k (figure 12*a–e*). In figure 12(*b*), unstable modes caused by resonance between equatorial Kelvin modes and continuous modes still exist near the dispersion curve of equatorial Kelvin modes (light blue line). (In figure 12(*b*), only one unstable mode appears at $k \approx 0.01$. However, it can be considered that more unstable modes actually exist near the light blue line in the small k region, since more unstable modes are obtained in supplemental calculation with 512 grids in the y-direction.) Contrary to this, in figures 12(*c*)–12(*e*), no unstable mode emerges along the the dispersion curve of equatorial Kelvin modes, since the dispersion curve of equatorial Kelvin modes exists below those of continuous modes. For $\log E = 1.20$ (figure 12*f*) at which symmetric inertially unstable modes appear, a root of $Q^3 - R^2 = 0$ for $n = 0$ is $k = 0$. The dispersion curves of equatorial Kelvin modes and westward mixed Rossby–gravity modes combine into one dispersion curve over the entire range of k to generate

unstable modes (green line) and decaying modes (figures not shown). This discussion is consistent with the result that neutral modes cannot be extracted for distorted basic flows in which continuous modes are excluded for values of $\log E \gtrsim 1.00$ (§ 5.2). For larger values of E (figure 12*g–h*), only the resonance between equatorial Kelvin modes and westward mixed Rossby–gravity modes emerges.

The intersections of the dispersion curves of equatorial Kelvin modes and westward mixed Rossby–gravity modes can be observed more clearly in the $(\log E, c)$-plane with fixed k (figure 13). Figure 13(*a*) shows the approximate dispersion curves (blue line) of equatorial Kelvin modes given by equation (5.5) and the numerically obtained dispersion curves on the $(\log E, c)$-plane for $k = 0.01$. (Isolated two unstable modes near $c \sim 5.0$ at $\log E \sim 1.40$ and $\log E \sim 1.80$ are spurious modes caused by numerical errors. These modes do not emerge in supplementary calculation with the domain of $-2 \leqslant y \leqslant 5$.) For $-1.00 \lesssim \log E \lesssim 1.20$, equatorial Kelvin modes resonate with continuous modes, which causes unstable modes. For $\log E \gtrsim 1.20$, the dispersion curve of equatorial Kelvin modes intersects that of westward mixed Rossby–gravity modes, and the resonance of these neutral waves causes instability. This type of resonance occurs at $\log E \approx 1.00$ for cases of larger k (figure 13*b*, *c*). As described above, by observing dispersion curves on the $(\log E, c)$-plane, it can be shown more clearly that zonally non-symmetric unstable modes for $\log E \gtrsim 1.20$ are caused by the resonance between equatorial Kelvin modes and westward mixed Rossby–gravity modes.

The modes whose dispersion curves exist near light blue line have been identified as equatorial Kelvin modes, although their dispersion curves are considerably distorted (especially, figures 12*d* and 12*e*). The distortion of the dispersion curve is considered to result from the occurrence of instability at the large k region. Simultaneously, the occurrence of instability deforms the structure of equatorial Kelvin modes. Figure 14 shows the structure of the neutral mode with $k = 0.005, c = -1.90$ in figure 12(*d*) ($\log E = 1.16$). Although the modes certainly have a Kelvin-wavelike structure to the south of the dynamic equator, the structure of the westward mixed Rossby–gravity wave can also be observed to the north of dynamic equator. This suggests that equatorial Kelvin modes are deformed and have features of the westward mixed Rossby–gravity wave because of instability at the large k region. The deformed equatorial Kelvin modes emerge as $n = 0$ modes in the uniform Γ-plane approximation.

7. Summary and discussion

An eigenvalue problem for a linear shear flow in a shallow-water system on an equatorial β-plane is solved over a wide range of values of E. For $\log E \lesssim 1.20$, only zonally non-symmetric unstable modes exist. The most unstable modes for $\log E \lesssim 1.00$ are caused by the resonance between equatorial Kelvin modes and continuous modes. The most unstable modes for $1.00 \lesssim \log E \lesssim 1.20$ are caused by the resonance between equatorial Kelvin modes and westward mixed Rossby–gravity modes. For $1.20 \lesssim \log E \lesssim 2.00$, the most unstable modes have zonally non-symmetric structures, although zonally symmetric unstable modes also appear. The most unstable modes are caused by the resonance between equatorial Kelvin modes and westward mixed Rossby–gravity modes. For $\log E \gtrsim 2.00$, zonally symmetric unstable modes are the most unstable. Other types of resonance occur, depending on the value of E: eastward mixed Rossby–gravity modes and continuous mode; eastward mixed Rossby–gravity modes and westward mixed Rossby–gravity modes; eastward inertial gravity modes and continuous modes; and eastward inertial gravity modes and

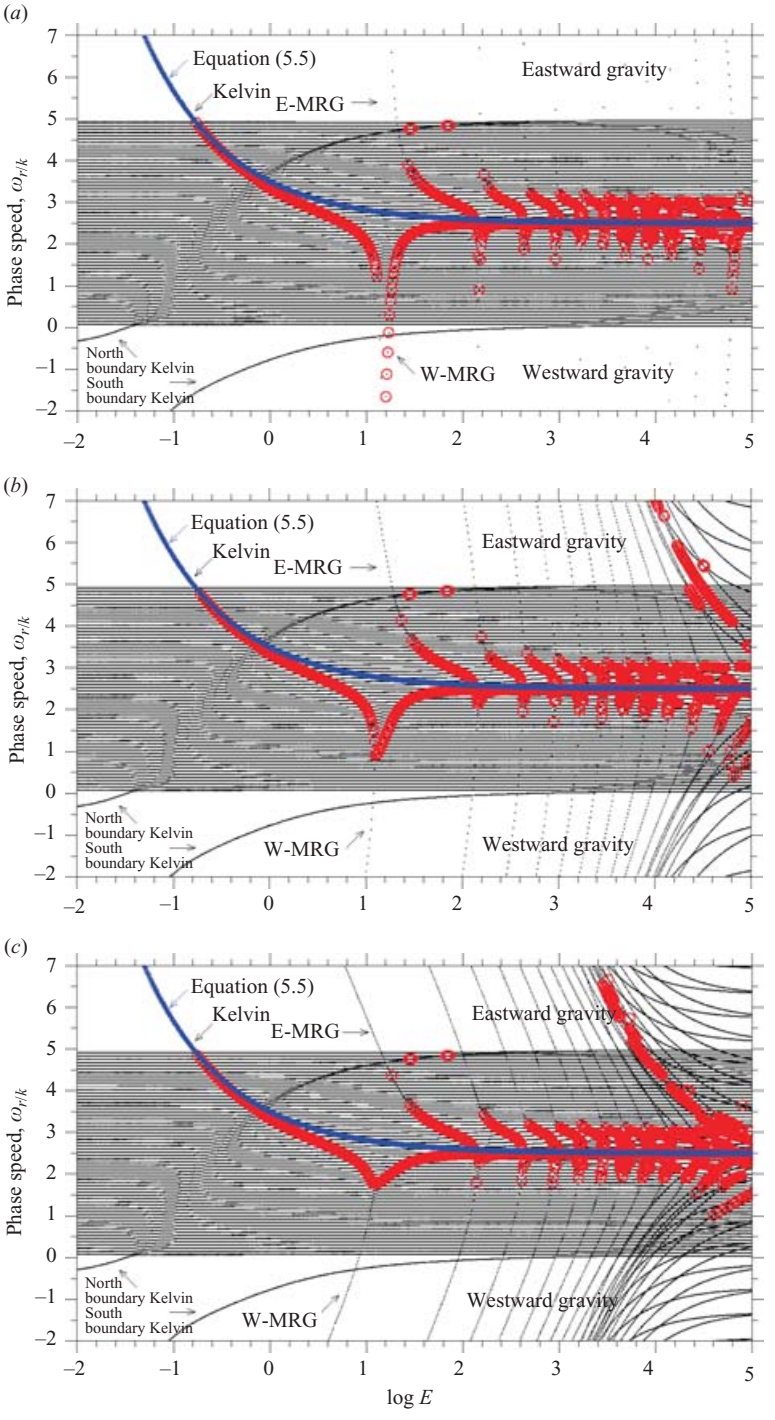

FIGURE 13. Dispersion curves on the $(\log E, c)$-plane for (*a*) $k = 0.01$, (*b*) $k = 0.05$ and (*c*) $k = 0.10$. Red circles and blue lines represent the unstable modes and the dispersion relation of equation (5.5), respectively.

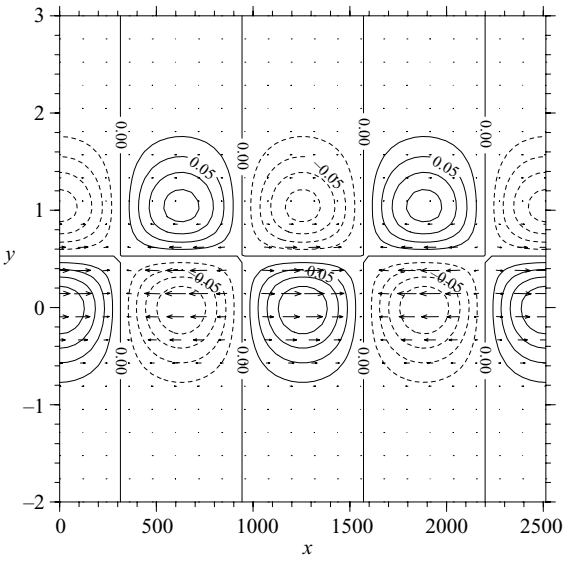

FIGURE 14. Horizontal structure of numerically obtained neutral mode (corresponds to light blue line in figure 12*d*) for $\log E = +1.16$, $k = 0.005$, $c = -1.90$. Contours and vectors indicate ϕ and the velocity field, respectively. Contour interval is 0.025.

westward inertial gravity modes. Although equatorial Rossby modes do not emerge in our discussions, equatorial Rossby modes actually exist. All equatorial Rossby modes are considered to assimilate into continuous modes, since detailed observations of mode structures show that some continuous modes have Rossby wavelike structure (figures not shown).

The zonally symmetric unstable modes obtained for $\log E > 1.20$ are inertially unstable modes discussed by Stevens (1983). In figures 12*f*–12*h*, it seems that the unstable modes with $k = 0$ exist on the dispersion curves of non-symmetric unstable modes caused by the resonance between equatorial Kelvin modes and westward mixed Rossby–gravity modes. This suggests that the instability caused by the resonance between these two neutral waves is the same kind of inertial instability. Although modes with $k = 0$ cannot be drawn on the (k, c)-plane, the connection of the dispersion curves of non-symmetric modes to symmetric modes can be examined on the (k, ω_r)-plane. Figure 15 shows the dispersion relations $\omega_r(k)$ for $\log E = 1.30$. The unstable mode of $k = 0$ certainly exists on the dispersion curve of the most unstable modes caused by the resonance between equatorial Kelvin modes and westward mixed Rossby–gravity modes. In addition, the approximate complex frequency of this non-symmetric unstable mode given by equation (6.12) coincides with that obtained by Stevens (1983) if $k \to 0$. Therefore, the non-symmetric unstable modes caused by the resonance between equatorial Kelvin modes and westward mixed Rossby–gravity modes, which are identical to the unstable modes obtained by Boyd & Christidis (1982) and Dunkerton (1983), can be considered to be the same kind of instability as the inertially unstable modes obtained by Dunkerton (1981) and Stevens (1983). The result that non-symmetric unstable modes for $\log E \gtrsim 1.20$ connect with symmetric modes is consistent with that of asymptotic expansion by Clark & Haynes (1996). The non-symmetric modes caused by the resonance between equatorial Kelvin modes and westward mixed Rossby–gravity modes can be considered to correspond to non-symmetric modes obtained by Clark & Haynes (1996).

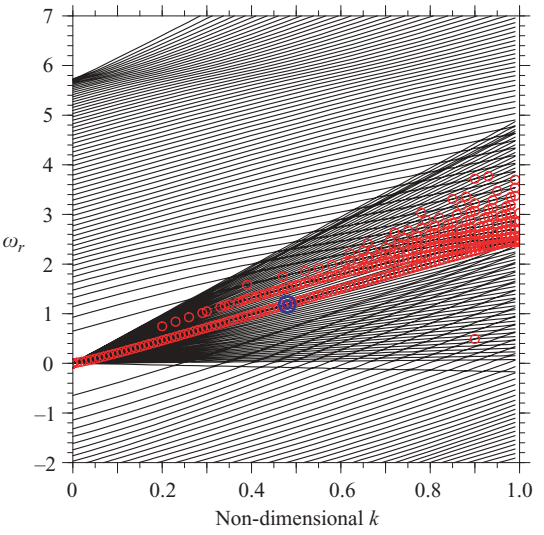

FIGURE 15. Dispersion curves for $\log E = 1.30$ on the (k, ω_r)-plane. Single red circles and double blue circles indicate unstable modes and the most unstable modes, respectively.

Our discussions using the concept of resonance of neutral waves does not give any conclusion that contradicts the results obtained by the ordinary instability theory. As for energetics of unstable modes, in the ordinary instability theory, it is often argued that disturbances gain their energy from the shear of mean flow. For resonance of neutral waves, energetics of unstable modes is described in terms of pseudoenergy. Pseudoenergy (or disturbance energy; Hayashi & Young 1987) is defined as the amount of energy in the fluid when the mode is excited minus the amounts in the unperturbed state, or in other words, the sum of the wave energy and that in the modified mean flow. Therefore, exchange of pseudoenergy is just another view of energy transfer from basic flow to growing disturbance. The additional results obtained by introducing the concept of resonance are a unified view for many kinds of unstable modes, the classification and the identification of unstable modes, which are supplements to the ordinary instability theory.

It remains to be solved whether pancake structures observed in the terrestrial middle atmosphere can be identified as inertial instability. Griffiths (2003) shows that the large vertical wavelength of observed pancake structures cannot be obtained by linear modes in a shallow-water system. This suggests that the results of the shallow-water model cannot be applied directly to an observed pancake structure. Griffiths (2003) points out the importance of a secondary Kelvin–Helmholtz instability. Examination for correspondence of unstable modes obtained in this paper to pancake structure requires reconsideration of the unstable modes in a three-dimensional system with the effect of Kelvin–Helmholtz instability, dissipation, and other effects. Further investigation is necessary in order to describe pancake structure in terms of linear unstable modes.

Our results show that many kinds of instability appear in the equatorial region. The type of mode that is most unstable and the induced circulation structure change according to external parameters. A change in E means a change in β if other parameters are fixed. Consequently, types of instability other than those observed in the terrestrial atmosphere can be discovered in the atmospheres of planets with

rotation rates different from that of Earth. Venus has a low rotation rate, and its atmosphere may be in a situation corresponding to cases of large E. If this is the case, zonally symmetric inertially unstable modes would tend to occur in the Venusian atmosphere. On the other hand, atmospheres on rapidly rotating planets such as Jupiter may be in a situation of small E. On Jovian planets, unstable modes due to the resonance between equatorial Kelvin modes and continuous modes can be discovered.

Several methods are used in this paper to identify resonating neutral waves. Among these, the calculation using basic flows with uniform velocity regions seems to be the most effective for extracting neutral modes. By excluding continuous modes, the resonating waves can be deduced: equatorial Kelvin modes and continuous modes for $\log E < 1.00$, and equatorial Kelvin modes and westward mixed Rossby–gravity modes for $\log E \gtrsim 1.00$. However, it has not been proved theoretically that continuous modes can be excluded and neutral modes can be extracted using distorted basic flows that have a uniform velocity region on an equatorial β-plane. We anticipate that the problem can be solved in a manner similar to the proof of the theorem in Lin (1945). We expect that the exclusion of continuous modes with distorted basic flows will be effective for identifying resonating waves not only for an equatorial β-plane, and that other kinds of unstable modes can be interpreted using the concept of resonance between neutral waves.

The authors wish to express their thanks to the anonymous reviewers for valuable comments on the original manuscript. The LAPACK library (http://www.netlib.org/lapack/) was used for solving the eigenvalue problems and the GFD-DENNOU library (http://www.gfd-dennou.org/arch/dcl/) was used for drawing the figures. This work is based in part on H. T.'s PhD dissertation at Hokkaido University.

REFERENCES

Allison, M., Del Genio, A. D. & Zhou, W. 1994 Zero potential vorticity envelopes for the zonal-mean velocity of the Venus/Titan atmospheres. *J. Atmos. Sci.* **51**, 694–702.

Allison, M., Del Genio, A. D. & Zhou, W. 1995 Richardson number constraints for the Jupiter and outer planet wind regime. *Geophys. Res. Lett.* **22**, 2957–2960.

Boyd, J. P. 1978 The effects of latitudinal shear on equatorial waves. Part I: theory and methods. *J. Atmos. Sci.* **35**, 2236–2258.

Boyd, J. P. & Christidis, Z. D. 1982 Low wavenumber instability on the equatorial beta-plane. *Geophys. Res. Lett.* **9**, 769–772.

Cairns, R. A. 1979 The role of negative energy waves in some instabilities of parallel flows. *J. Fluid Mech.* **92**, 1–14.

Clark, P. D. & Haynes, P. H. 1996 Inertial instability on an asymmetric low-latitude flow. *Q. J. R. Met. Soc.* **122**, 151–182.

Dunkerton, T. J. 1981 On the inertial stability of the equatorial middle atmosphere. *J. Atmos. Sci.* **38**, 2354–2364.

Dunkerton, T. J. 1983 A nonsymmetric equatorial inertial instability. *J. Atmos. Sci.* **40**, 807–813.

Dunkerton, T. J. 1993 Inertial instability of nonparallel flow on an equatorial β plane. *J. Atmos. Sci.* **50**, 2744–2758.

Griffiths, S. D. 2003 Nonlinear vertical scale selection in equatorial inertial instability. *J. Atmos. Sci.* **60**, 977–990.

Hayashi, H., Shiotani, M. & Gille, J. C. 1998 Vertically stacked temperature disturbances near the equatorial stratopause as seen in cryogenic limb array etalon spectrometer data. *J. Geophys. Res.* **103**, 19 469–19 483.

Hayashi, Y.-Y. & Young, W. R. 1987 Stable and unstable shear modes on rotating parallel flows in shallow water. *J. Fluid Mech.* **184**, 477–504.

Hitchman, M. H., Leovy, C. B., Gille, J. C. & Bailey, P. L. 1987 Quasi-stationary zonally asymmetric circulations in the equatorial lower mesosphere. *J. Atmos. Sci.* **44**, 2219–2236.

Iga, K. 1993 Reconsideration of Orlanski's instability theory of frontal waves. *J. Fluid Mech.* **255**, 213–236.

Iga, K. 1995 Transition modes of rotating shallow water waves in a channel. *J. Fluid Mech.* **294**, 367–390.

Iga, K. 1997 Instability of a front with a layer of uniform potential vorticity. *J. Met. Soc. Japan* **75**, 1–11.

Iga, K. 1999*a* Critical layer instability as a resonance between a non-singular mode and continuous modes. *Fluid Dyn. Res.* **25**, 63–86.

Iga, K. 1999*b* A simple criterion for the sign of the pseudomomentum of modes in shallow water systems. *J. Fluid Mech.* **387**, 343–352.

Iga, K. 1999*c* Unstable wave as a resonance between waves. *Mathematical Aspects on Waves of Strong Nonlinearity or Large Degree of Freedom (ed. M. Funakoshi) (RIMS Kokyuroku)* **1092**, 57–67 (in Japanese).

Iga, S. & Matsuda, Y. 2005 Shear instability in a shallow water model with implications for the Venus atmosphere. *J. Atmos. Sci.* **62**, 2514–2527.

Kubokawa, A. 1986 Instability caused by the coalescence of two modes of a one-layer coastal current with a surface front. *J. Oceanogr. Soc. Japan* **42**, 373–380.

Kuo, H. L. 1949 Dynamic instability of two-dimensional non-divergent flow in a barotropic atmosphere. *J. Met.* **6**, 105–122.

Lin, C. C. 1945 On the stability of two-dimensional parallel flows. Part II. *Q. Appl. Maths.* **3**, 218–234.

Matsuno, T. 1966 Quasi-geostrophic motions in the equatorial area. *J. Met. Soc. Japan* **44**, 25–43.

Natarov, A. & Boyd, J. P. 2001 Beyond-all-orders instability in the equatorial Kelvin wave. *Dyn. Atmos. Ocean.* **33**, 191–200.

Stevens, D. E. 1983 On symmetric stability and instability of zonal mean flows near the equator. *J. Atmos. Sci.* **40**, 882–893.

Winter, Th. & Schmitz, G. 1998 On divergent barotropic and inertial instability in zonal-mean flow profiles. *J. Atmos. Sci.* **55**, 758–776.